Journal of the Meteorological Society of Japan, Vol. 76, No. 5, pp. 799–815, 1998

Variation of Summer Water Vapor Transport Related to Precipitation over and around the Arid Region in the Interior of the Eurasian Continent

By Akiyo Yatagai[1]

National Space Development Agency of Japan, Earth Observation Research Center (NASDA/EORC), 1-9-9 Roppongi, Minato-ku, Tokyo 106-0032, Japan

and

Tetsuzo Yasunari

Institute of Geoscience, University of Tsukuba, Ibaraki 305-8571, Japan

(Manuscript received 15 November 1996, in revised form 5 August 1998)

Abstract

The variability of the hydrological cycle for arid/semi-arid regions is important, because desertification is occurring in these regions. Even in the arid/semi-arid regions in the interior of the Eurasian Continent, heavy precipitation sometimes occurs. However, the relationship between water vapor transport and precipitation has not been clarified yet.

In this study, water vapor transport and flux divergence in the arid interior region of the Eurasian Continent were investigated using the objective re-analysis data provided by the European Centre for Medium range Weather Forecast (ECMWF) for a five-year period (1980–1984). Through the analysis of the vertically integrated water vapor transporting mean summer fields, it is clarified that Mongolia and the northern part of China receive water vapor from the northwest. One of the water sources for these regions is located over, and to the west of Western Siberia. In the lower troposphere, most of the water vapor is transported to the Taklimakan Desert from the northwest along the eastern periphery of the Tianshan Mountains in the mean summer state.

The daily summer water vapor flux fields around the Taklimakan Desert for a five-year period were analyzed in relation to precipitation there. The Taklimakan Desert is one of the most arid regions in the Eurasian Inner Continent. Here, the daily mean water vapor flux patterns are classified using cluster analysis. The 460 maps prepared during the investigation are first classified into eight general patterns. Precipitation and atmospheric circulation patterns compositted by these clusters are then compared. Over 90 % of the total cases resemble the summer mean water vapor flux pattern, and northwesterly moisture flows prevail.

We found that the southerly water vapor flows, which pass over the Tibetan Plateau and along the eastern periphery of the Plateau in the lower level, are related to heavy precipitation over the Taklimakan Desert. The simultaneous existence of a southwestward extending trough located to the north of this region, and the ridge located in Central Asia, is peculiar to the atmospheric circulation pattern of these cases. Although such situations appeared in up to 10 % of the total cases, they tend to occur mostly in the wet years (1981, 1984), and account for about half of the precipitation in those wet years.

1. Introduction

Even in the desert in the interior of the Eurasian Continent, heavy rainfall sometimes occurs (Yoshino, 1991). How is the water vapor provided to produce such rainfall events? The variation of the precipitation amount over there is likely to be influenced by both monsoon circulation and the mid-latitude westerly circulation in the summertime.

Many studies deal with water vapor transport on Asian monsoons (*e.g.*, Asakura, 1973; Yoshino and Chen, 1975; Murakami *et al.*, 1984) and on Bai-u (Mei-yu) (*e.g.*, Murakami, 1959; Akiyama, 1973).

1 Corresponding author: Akiyo Yatagai, National Space Development Agency of Japan, Earth Observation Research Center (NASDA/EORC), 1-9-9 Roppongi, Minato-ku, Tokyo 106-0032, Japan. E-mail: yatagai@eorc.nasda.go.jp

These studies have shown three major routes of water vapor transport over Asia during the summer monsoon season: 1) Southwesterly flow through India and China, 2) Southeasterly flow around the western edge of the Pacific High, and 3) Northwesterly flow from Siberia. The arid and semi-arid regions over China and Mongolia are likely to be directly influenced by both flow 1), which is related to South and East Asian summer monsoons, and flow 3), which is related to mid-latitude westerlies, in summertime.

However, due to a lack of aerological data over the arid and semi-arid regions, few studies have dealt with water vapor transport in these areas, and they yielded very ambiguous results. Zhang and Deng (1987) summarized the precipitation and its related phenomena over Xinjiang Province. Kato *et al.* (1992) and Kato (1993) investigated the land-surface processes and water cycles around the arid regions of China during the 1985 warm season. Kato (1995) summarized the recent studies of the large to middle-scale phenomena over Northwest China. Though these studies dealt with water vapor transport as case studies, a statistical approach has not yet been done. Thus it is necessary to analyze water vapor transport statistically to understand the relationship between precipitation, moisture transport and the atmospheric circulation pattern.

Recently, Kitoh *et al.* (1993) described the summertime moisture flux climatology over Northwest China by using the objective analysis data provided by the National Meteorological Center (NMC, the present name is National Centers for Environmental Prediction (NCEP)). They clarified the main difference of mean moisture circulation between the Taklimakan and Gobi Deserts. However, the moisture transportation field related to precipitation has not been studied. Yatagai and Yasunari (1993) investigated the relationship between precipitation and water vapor transport around the arid and semi-arid regions of China, by using the objective analysis data of the European Centre for Medium Range Weather Forecast (ECMWF). However, dynamic characteristics relating to each precipitation event have not been clarified, and interannual variability was not investigated.

Since the First Global Atmospheric Research Programme (GARP) Global Experiment (FGGE) year, 1979, objective analysis has been performed to provide data yielding initial values for numerical weather forecasting, based on optimization of observational data by using the Numerical Weather Prediction (NWP) Model (Bengtsson *et al.*, 1982). These products were affected by changes in the NWP model as well as other modifications of the four-dimensional data assimilation (4DDA) scheme. To reduce these effects, re-analysis efforts have recently been made, and the re-analysis data set has recently become available. It uses a frozen state-of-the-art analysis and forecast system and performs data assimilation using past data to the present. It is thus very useful for researches on climate change, although the change of input data should be monitored closely. In this study, we use the ECMWF re-analysis data to discuss the interannual variability of the water vapor flux field.

The purpose of this study is to clarify the interrelationships between water vapor transport, atmospheric circulation and heavy precipitation over the arid and semi-arid regions of China and Mongolia. To better understand the relationship between water circulation and climatic change, water vapor flux is an interesting physical quantity because it is reflected in the atmospheric circulation pattern and is closely related to precipitation phenomena. As mentioned above, there have been many case studies about the relationship between precipitation and atmospheric circulation fields. However there is little precipitation over arid regions, and it occurs sporadically. As a result, a statistical approach of water circulation based on precipitation over a large-scale arid region may be limited. In this study, water vapor flux patterns are classified, then they are compared with precipitation and atmospheric circulation patterns.

The controlling factor and mechanisms of precipitation variability may differ from area to area. In this study, we particularly focus on the Taklimakan Desert and a part of the Gobi Desert, which are located at the center of the widely distributed dry regions in the interior of the Eurasian Continent. The interannual variability of summer precipitation there shows a regionality. Namely, time series of precipitation of the stations in those areas show high positive correlation each other (Yatagai and Yasunari, 1995).

The focused area is one of the driest region in the interior of the Eurasian Continent. In most parts of Mongolia and North and Northwest China, except for the north of the Tianshan Mountains, more than 50 % of the annual total precipitation occurs in summer. To the north of the Tibetan Plateau and in most parts of Mongolia, summer precipitation accounts for more than 70 % of the annual precipitation (Yatagai and Yasunari, 1995).

The names of major geographical regions used in this study can be seen in the Appendix of Yatagai and Yasunari (1995).

2. Data and analysis method

The objective re-analysis data produced by the ECMWF 4DDA system were used for the period from 1980 to 1984. The temporal resolution is four times a day (00, 06, 12 and 18 UTC), and the horizontal resolution is 2.5° × 2.5° (longitude/latitude) grids. The original horizontal resolution of the NWP

model used at ECMWF to make this dataset was T106. The data used here are the geopotential height (z), zonal and meridional winds ($\vec{V}(u, v)$), temperature (T), and relative humidity (Rh) at seventeen standard pressure levels (1000, 925, 850, 775, 700, 600, 500, 400, 300, 250, 200, 150, 100, 70, 50, 30 and 10 hPa) on each grid point.

The precipitable water (W) and vertically integrated horizontal flux vector of water vapor ($\vec{Q}$) were calculated by:

$$W = \frac{1}{g}\int_{10\ \mathrm{hPa}}^{Ps} q dP \tag{1}$$

and

$$\vec{Q} = \frac{1}{g}\int_{10\ \mathrm{hPa}}^{Ps} q\vec{V} dP, \tag{2}$$

where q, g, and Ps represent specific humidity, acceleration due to gravity and pressure at ground surface, respectively. Specific humidity is calculated from the temperature and relative humidity by Goff-Gratch's equation (Goff and Gratch, 1946). The determination of Ps was adopted in the method of Oki *et al.* (1995), and vertically integrated water vapor flux was computed. Since q is very small in the upper troposphere through the stratosphere, water vapor flux over 10 hPa can be neglected. Over and leeward of the Tibetan Plateau, q and the water vapor flux of the upper troposphere are not negligible. $\vec{Q}$ corresponds to the total water vapor flux. Areal ($2.5° \times 2.5°$) mean water vapor flux divergence or convergence is computed using Gauss's theorem,

$$\int_S div\vec{Q} ds = \int_\Gamma \vec{Q}\cdot\vec{n} dl, \tag{3}$$

where S is the area surrounded by the adjacent four grid points. Γ is the boundary of the region, $\vec{n}$ is the outward unit normal vector, and dl is the element of length along the boundary.

The liquid water and its flux divergence in the atmosphere can be neglected except over coastal upwelling regions (*e.g.*, Bryan and Oort, 1984). Thus the balance equation for atmospheric water is

$$\frac{\partial W}{\partial t} + div\vec{Q} = E - P, \tag{4}$$

where E is the evaporation from the surface and P is the precipitation amount falling on the surface. If the time tendency of W (the first term) is very small, divergence (convergence) of $\vec{Q}$ corresponds to the source (sink) regions.

In this study, the vertically integrated water vapor flux for the lower troposphere is also defined as

$$\vec{Q}_L = \frac{1}{g}\int_{700\ \mathrm{hPa}}^{Ps} q\vec{V} dp. \tag{5}$$

These quantities were computed for every 6-hour period. Daily, monthly and seasonal (June, July, August, hereafter denoted as JJA) mean values were then obtained.

Precipitation amount data used in this study were derived from global daily summary (GDS) datasets compiled by the National Oceanic and Atmospheric Administration/National Climatic Data Center (NOAA/NCDC). The data used for this dataset were initially received over the Global Telecommunications System (GTS) by the NMC, then archived at the NCDC.

3. Mean water vapor flux and its divergence field

The vertically integrated summer mean water vapor flux is shown in Fig. 1 for (a) the whole layer and (b) the lower troposphere. The shaded region in Fig. 1a represents convergence. A northwesterly flow prevails over the arid and semi-arid regions in the interior of the Eurasian Continent (40–50°N/60–110°E). It converges with the southerly flow around 35°N/110°E. The overall feature shows that the water vapor flowing to the arid and semi-arid regions of China and Mongolia comes from the north or northwest direction. Therefore, one of the water sources to the arid and semi-arid regions may be located over, and to the west of Western Siberia. The central part of the Taklimakan Desert shows water vapor flux divergence, whereas the eastern foot of Pamir shows convergence. A weak convergence is spread over most parts of the Tibetan Plateau, and the eastern part of Taklimakan Desert. In the lower troposphere, water from the north seems to flow around the east of the Tianshan Mountains and converge there, and then flow over the Taklimakan Desert. Water vapor flux is not clear over North China.

The overall flux patterns are very similar to those computed from the ECMWF operational dataset (Yatagai and Yasunari, 1993) and from NMC (Kitoh *et al.*, 1993). However, the patterns of divergence and convergence shown here are somewhat different from those in the previous studies. Some convergence is apparent over Western Siberia in Fig. 1a (40–70°N/60–90°E), but was not seen in the previous results. The unrealistically strong divergence, which appeared over open seas and the Taklimakan Desert using the ECMWF operational dataset in the early 1980s, is not seen in Fig. 1a.

Figure 2 shows the five-year mean water vapor budget around the Taklimakan Desert for summer (JJA). Parts of the Tibetan Plateau and Tianshan Mountains are involved in this box. The four numerals in italics indicate the total water vapor transport that crosses each boundary of the box. The number in the box denotes the net budget in the box. A positive number represents convergence (income). The rate of time change of precipitable water may be neglected since this figure shows the long-term

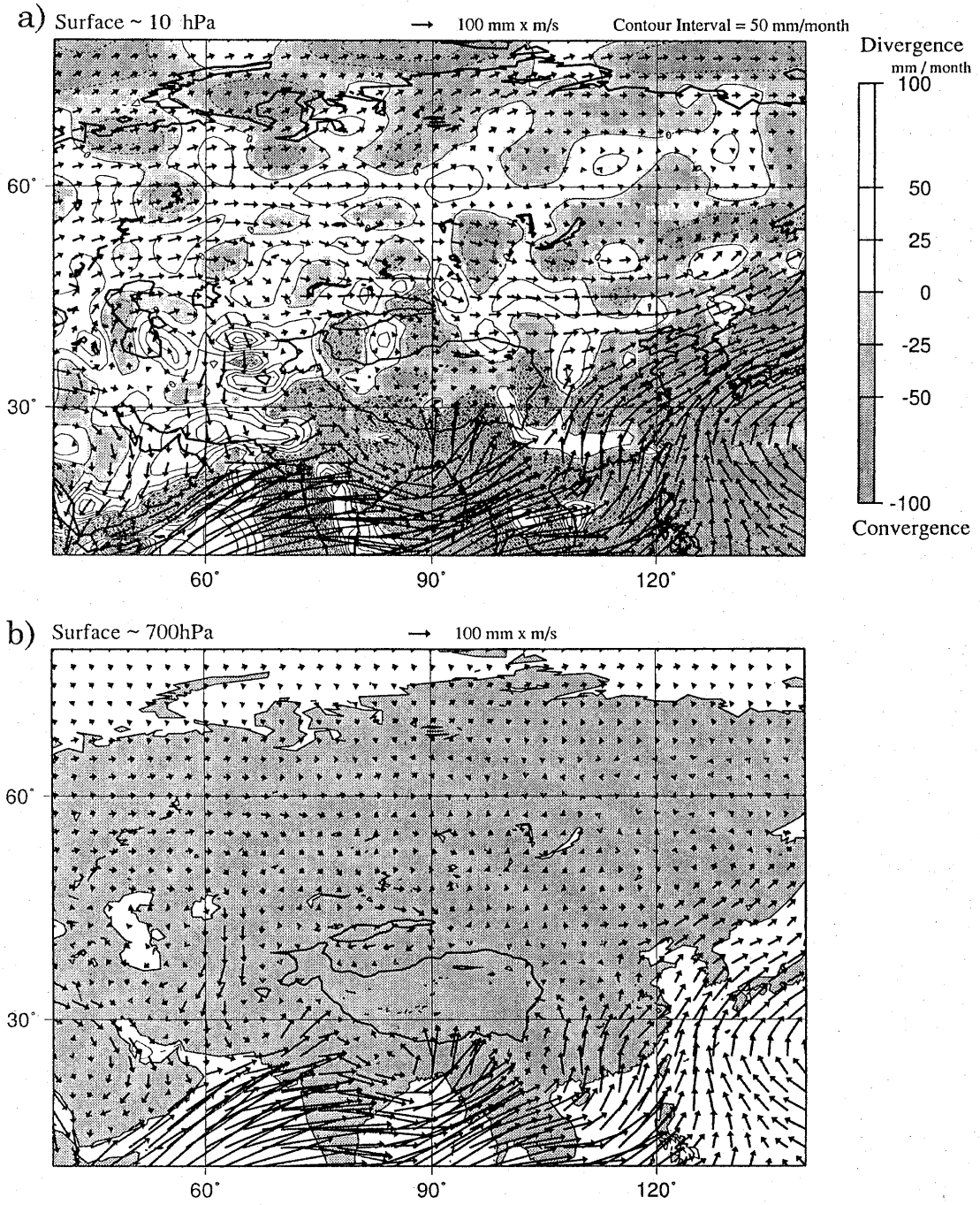

Fig. 1. Mean summer (JJA) water vapor transport calculated in a) the whole layer and b) the lower troposphere (up to 700 hPa). Water vapor flux divergence and convergence (shaded) are also shown in the upper panel. The Tibetan Plateau (contour of 3,000 m height) is represented by a thick full line. The thin full line in a) indicates divergence, while the thin dashed line shows convergence. Contour interval of divergence and convergence is 50mm/month.

mean. Water vapor comes in from the north, west and south, and goes out to the east. The northerly inflow is the largest among the three boundaries. The water vapor budget in this box indicates a weak convergence (1.5×10^{12} kg/day).

4. Water vapor flux related to heavy precipitation

In this study, we focus on the relationship between the large-scale water vapor flux pattern associated with large-scale atmospheric circulation, and precipitation variability. Since spatial and temporal precipitation variability is very large in the arid region, the regionality of precipitation should be considered for this purpose. Yatagai and Yasunari (1995) have shown that the summer precipitation in stations of the Taklimakan Desert exhibits a rather coherent interannual variation compared to other stations in

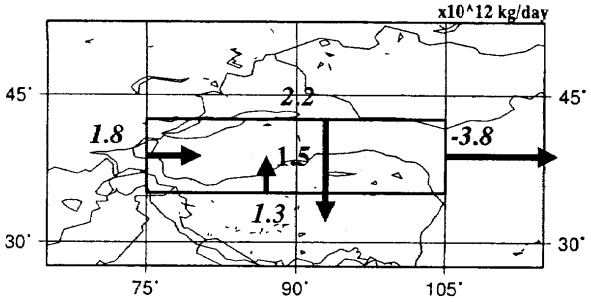

Fig. 2. The budget of mean summer water vapor flux around the Taklimakan Desert. Numbers in Italics indicate total inflow (or outflow) that crosses each boundary of the box. The number in the box denotes the net budget in the box. Unit is 10^{12} kg/day. The net budget value 1.5×10^{12} kg/day corresponds to 0.7 mm/day, since the area of the box is 2.2×10^{12} km^2.

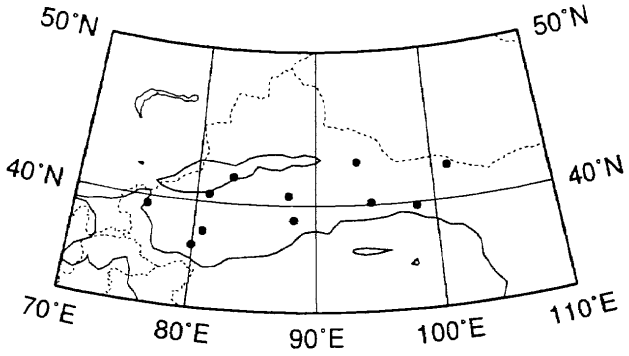

Fig. 3. Geographical distribution of the daily precipitation stations in Taklimakan Desert.

the widely-distributed arid and semi-arid regions in the interior of the Eurasian Continent. Therefore, we define the areal mean precipitation of 11 stations in the Taklimakan Desert as the "Taklimakan precipitation." The location of the 11 stations is shown in Fig. 3.

Figure 4 indicates the daily Taklimakan precipitation for 1980–1984 in summertime. The daily and seasonal mean Taklimakan precipitation of these five years are 0.3 mm and 30 mm, respectively. Here, we define a daily Taklimakan precipitation exceeding 3 mm as "heavy precipitation." Heavy precipitation for a few days contributes most of the monthly or seasonal precipitation. During the five years, heavy precipitation was observed on 11 days, and 1981 was a very wet year, especially in July and August. The sum of the 11 days precipitation occupies about 30 % of total precipitation for the 5-years' summer.

The composite water vapor flux pattern for the 11 days of heavy precipitation is shown in Fig. 5. It is interesting that a strong southerly flux is seen over the Tibetan Plateau in Fig. 5a. Around the

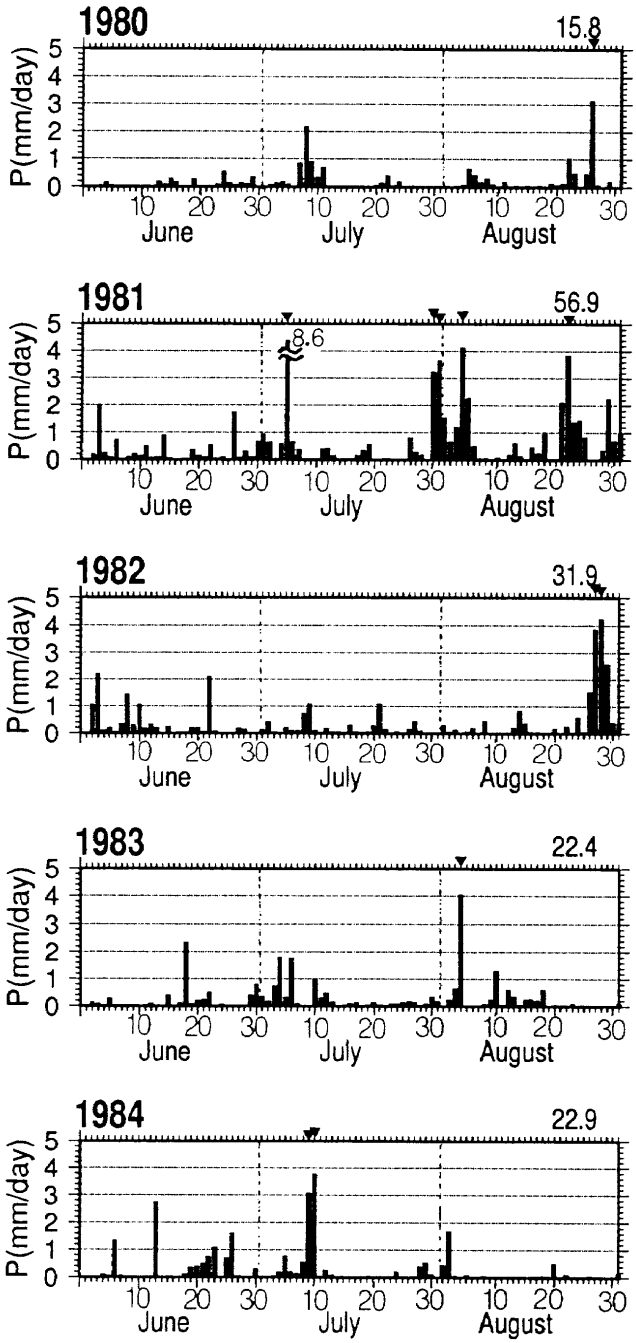

Fig. 4. Time series of Taklimakan precipitation for the summer of 1980–1984. Units are mm/day. Tick marks indicate the days of heavy Taklimakan precipitation. The numbers at the upper right of each graph indicate the total summer precipitation of each year.

Loess Plateau (103°N/40°E), most of the southerly water vapor in the lower level seems to flow into the desert from the east (Fig. 5b). Since the Tibetan Plateau exceeds 700 hPa in height, water vapor flux there is not computed in Fig. 5b. In Fig. 5a, a large southwesterly flux appears over the Tibetan Plateau and Gobi Desert, and it converges over Gobi and around 90°E/39°N. To the north of this re-

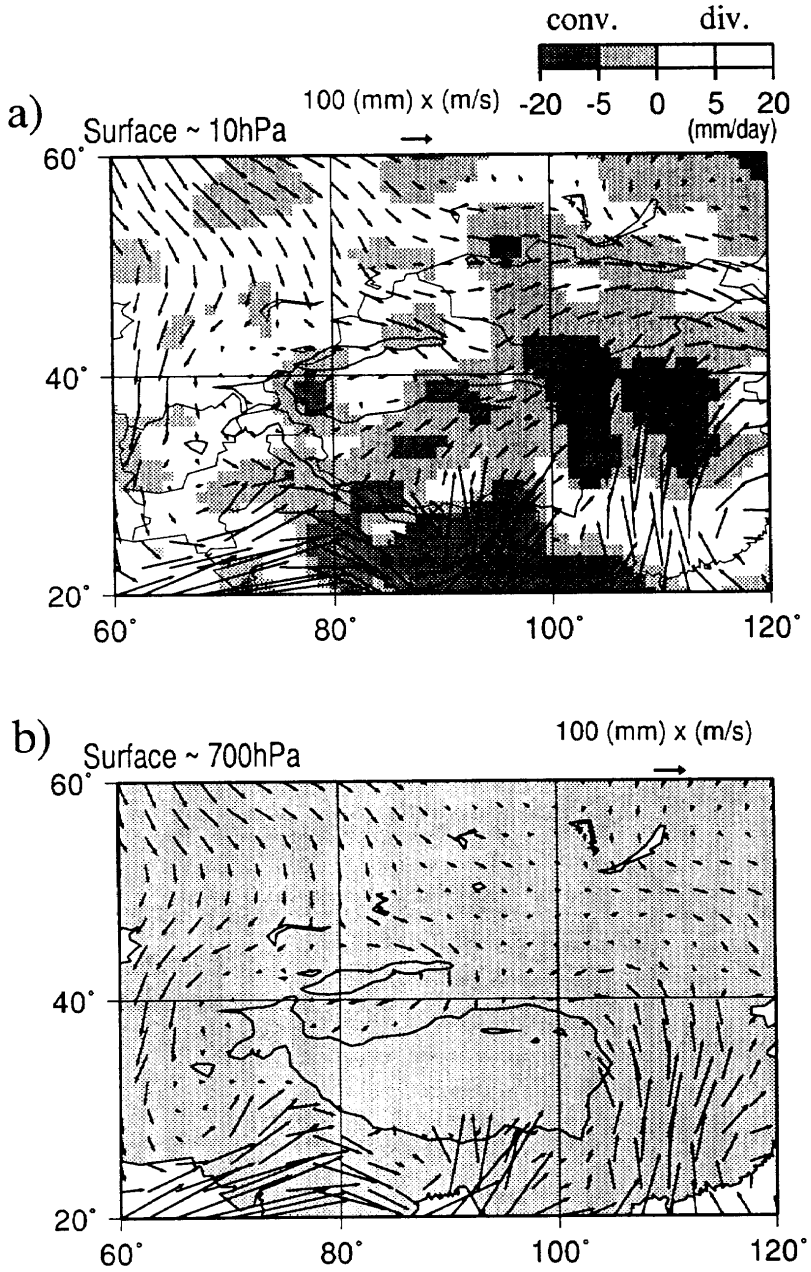

Fig. 5. Composite of water vapor flux pattern for the days of heavy Taklimakan precipitation (11 cases) for a) total water vapor flux. Shaded area indicates water vapor flux convergence. b) Same as a), but for the lower troposphere (up to 700 hPa).

gion (45–60°N/60–80°E), a large northerly flux is apparent. These patterns differ from those of the mean fields (Figs. 1a and 1b), especially over the Gobi Desert (around 42°N/100°E). The southwesterly flow over Tibet, which may bring moisture over or from the south of the Tibetan Plateau, may have not been pointed out yet. In Fig. 5b, a southerly flow from the south turns around the northeast of the Plateau. This feature of lower level flow seems to be related with the previous studies (*e.g.*, Yatagai and Yasunari, 1993). Details will be discussed in Section 6.

Comparing Fig. 5a with Fig. 5b, interesting features about the vertical structure can be pointed out. (1) Over Gobi Desert (105°E/40°N), a conspicuous difference is seen between the water vapor flux and convergence pattern. For the total moisture field, moisture flows northeastward, but at a lower level flux field, moisture flows westward and converges there. (2) East of the Tianshan Mountains (88°E/45°N), the moisture flow from the northwest to the Taklimakan Desert seems to be the same in Figs. 5a and 5b. Around 90°E/39°N, northwesterly flux and upper level moisture from the Tibetan Plateau seem to converge at the northern foot of the Tibetan Plateau. (3) Furthermore, the

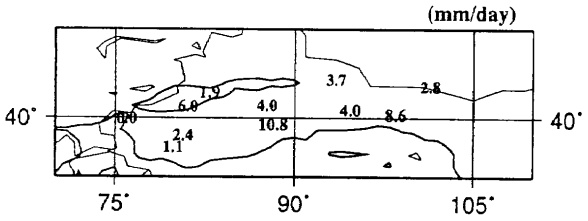

Fig. 6. Distribution of daily precipitation composite for the days of heavy Taklimakan precipitation.

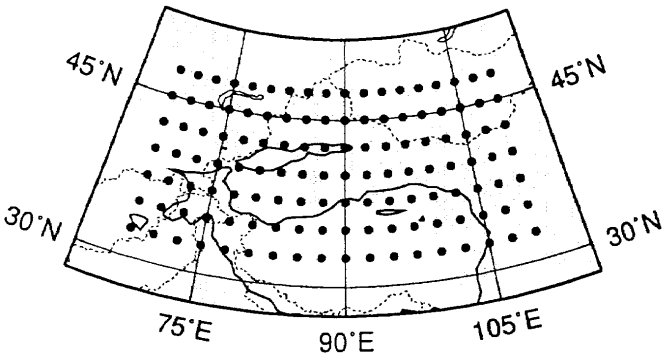

Fig. 7. The grid points where the water vapor flux is classified by cluster analysis.

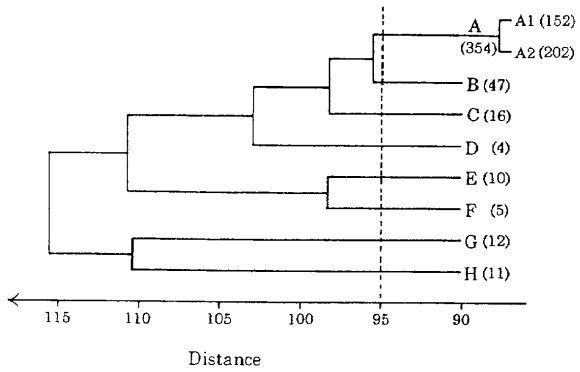

Fig. 8. Dendrogram represents the process of linkage of clusters. Letters denote the cluster types, and numerals in parenthesis are the number of cases for each cluster.

easterly moisture in the lower troposphere around 100°E/40°N may be related with the convergence around 90°E/39°N. This difference of the vertical structure of moisture convergence should be studied in the future.

Figure 6 shows the composite precipitation for 11 cases of heavy Taklimakan precipitation. Heavy precipitation observed at 89°E/39°N (10.8 mm/day) and 98°E/40°N (8.6 mm/day) corresponds to convergence, especially in the lower level at the northern foot of the Tibetan Plateau.

5. Variability of water vapor transport and precipitation over and around the Taklimakan Desert

In the previous sections, the water vapor transport pattern of the seasonal mean state and the composite of heavy rain cases have been presented. Relatively few days of precipitation may contribute to most of the seasonal precipitation in the arid and semi-arid regions. The atmospheric circulation and water vapor transport patterns related to the precipitation event seem to differ from case to case in such arid and semi-arid regions, because both southerly monsoon and westerly circulations may influence these regions. Therefore, to understand the relationship between water vapor transport patterns and precipitation, it is necessary to analyze daily water vapor flux patterns corresponding to daily precipitation. Since large-scale water vapor flux reflects global and synoptic circulation fields, analysis of the flux patterns may also manifest some important relationships between atmospheric circulation fields and heavy precipitation.

Daily total water vapor flux patterns around the Taklimakan Desert were classified using cluster analysis. The classified patterns were then compared with the precipitation distribution and the atmospheric circulation fields.

We preferred cluster analysis to other multivariate analysis (*e.g.* Empirical Orthogonal Function analysis) in classification because this method can extract relatively minor (rare case) patterns. Characteristics of classification patterns and their relationship to precipitation, atmospheric circulation fields, and their interannual variability are then described.

5.1 Classification method

The classification procedure using cluster analysis is described as follows. First, daily water vapor flux patterns for summer (JJA) days were computed for 1980–1984, as described in Section 2. In this study, total water vapor flux ($\vec{Q}(QU, QV)$) fields in the area shown in Fig. 7 are classified. A total of 460 patterns were classified by cluster analysis using the group average method, which is an agglomerative hierarchical technique defining all pairs of individuals in the two groups (Everitt, 1993).

D_{ab}, the distance between water vapor flux patterns 'a' and 'b,' is defined by the following equation:

$$D_{ab} = \frac{1}{N}\sum_{i=1}^{N}\sqrt{(QU_{ai} - QU_{bi})^2 + (QV_{ai} - QV_{bi})^2}, \tag{6}$$

where i represents each grid point of concern as shown in Fig. 7 and N denotes the number of grid points ($N = 126$). The zonal flux at grid 'i' on the pattern 'a' is given by QU_{ai}, while that for pattern 'b' is represented by QU_{bi}. QV_{ai} and QV_{bi} mean the same as QU_{ai} and QU_{bi}, but for the meridional flux. This equation is basically the same as the previous

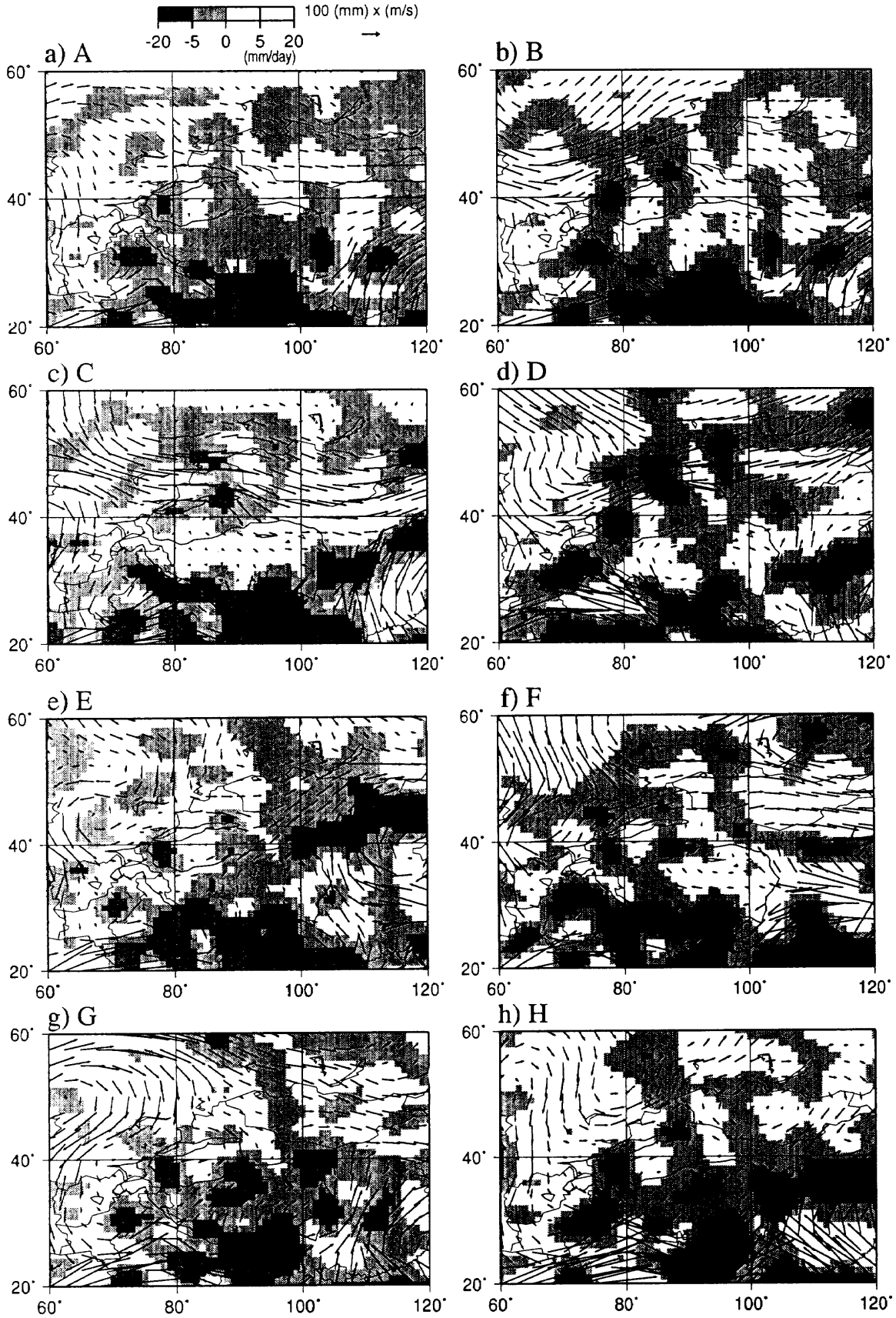

Fig. 9. The composite maps of water vapor flux patterns for clusters a) A, b) B, c) C, d) D, e) E, f) F, g) G and h) H. Shaded areas indicate convergence of water vapor flux.

Table 1. The number of occurrence for each cluster in each year and month.

Cluster	1980	1981	1982	1983	1984	June	July	Aug.	Sum
A	80	60	76	70	68	117	121	116	354
B	11	9	8	12	7	23	5	19	47
C	0	4	0	5	7	0	11	5	16
D	0	1	0	3	0	0	1	3	4
E	0	8	2	0	0	0	6	4	10
F	0	5	0	0	0	0	3	2	5
G	1	0	6	2	3	3	4	5	12
H	0	5	0	0	6	7	4	0	11
A1	29	17	38	36	32	39	70	43	152
A2	51	43	38	34	36	78	51	73	202

work applied to the wind field (*e.g.*, Tagami, 1982; Suzuki and Kawamura, 1987).

The individual water vapor flux patterns are linked with each other in clusters through the following procedure (Suzuki, 1990).

1. The distances between all the pairs of patterns (clusters) are calculated according to the definition in Eq. (6).
2. The pair of clusters that has the smallest distance is linked first and a new cluster is established.
3. The distance between the new cluster and other clusters is re-calculated according to the same definition.

Procedures 2 and 3 are repeated until the number of clusters decreases to one.

5.2 Classified water vapor flux patterns

The result of cluster analysis is displayed in Fig. 8 as a dendrogram. The vertical lines denote the hierarchy of clusters, and the horizontal lines indicate the distances at which a pair of clusters is linked. The classification is first performed at a distance of 95 in this dendrogram, and subsequently eight types of water vapor flux patterns are objectively deduced. The critical distance, which divides clusters, was synthetically defined based upon the number of cluster types and each composite pattern. It is noteworthy that a cluster consisting of a small number of cases can not be neglected because very rare and abnormal circulation may sometimes be responsible for heavy precipitation in this arid region as suggested in Section 4.

Cluster A includes 354 cases and accounts for 77 % of total cases as shown in Fig. 8. Therefore, cluster A is subdivided to two sub-clusters A1 and A2 by the distance. The former includes 152 cases, while the latter has 202 cases.

The composite maps of water vapor flux for each cluster pattern (A–H) are presented in Figs. 9a–9h. Two major moisture flows, related with westerly and monsoon circulations, can be seen in all the patterns. Cluster A has the largest number of cases as shown in Table 1. The composite water vapor flux pattern (Fig. 9a) resembles the seasonal mean flux pattern shown in Fig. 1a. It should be pointed out that in Figs. 9e and 9g, strong moisture flux from the south over the Tibetan Plateau appears.

The numbers of occurrence of each cluster in each year and month are shown in Table 1. The Taklimakan precipitation for each cluster pattern is shown in Fig. 10. This figure shows that the average precipitation amounts of clusters E, G and H are very large compared to the others.

The 11 heavy precipitation cases discussed in the previous section are classified clusters A1, A2, B, E, G and H. Details are shown in Table 2. This table shows that five cases of heavy precipitation are included in A1, A2 and B, which do not show much precipitation on average. Nearly half of the heavy precipitation cases are included in A and B, which somewhat resemble the pattern for the mean state. These results indicate that the relationship between the water vapor transporting field and precipitation is not so simple. However, we can say that the clusters related with the strong moisture from the south such as clusters E, G and H are related to heavy precipitation. Interestingly, appearance of classified clusters related to heavy precipitation seems to differ from year to year. Clusters G and H occur in 1981 and 1984, whereas A1, A2 and B occur in 1980, 1982, 1983 and only one case (August 22) in 1981. The heaviest case, July 5, 1981 is included in H. Thus, features of year-to-year difference of occurrences of water vapor flux cluster patterns may be affected by the differences of seasonal mean atmospheric circulation pattern.

Figure 11 shows composites of precipitation patterns of the cluster a) A, b) E, c) G and d) H. All stations in Fig. 11a show little composite precipitation. Heavy precipitation areas, which appear in E, G, and H, are different among one another. De-

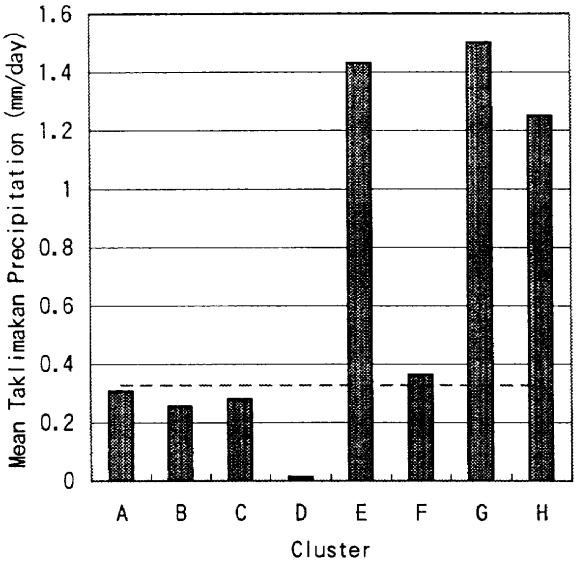

Fig. 10. Daily Taklimakan precipitation for each cluster. The dashed line denotes the mean of daily precipitation (0.3 mm/day).

tails are discussed with the atmospheric circulation patterns.

In order to examine the contribution of precipitation caused by each cluster, precipitation explained by each cluster is presented in Fig. 12b. For comparison, number of days classified for each cluster is presented in Fig. 12a, which is substantially the same as Table 1. As mentioned before, 1981 was a very wet year. It is clear that precipitation in the summer of 1981 was characterized basically by the patterns of the remarkable southerly flux over the Tibetan Plateau, corresponding to clusters E, F and H. In 1980, 1982 and 1983, the rate of precipitation related to cluster A is relatively high, while clusters E, F, G and H for 1981 and 1984 contribute about half of the total precipitation. It is also noteworthy that in some years (*e.g.*, 1980 and 1983) these clusters seldom appear.

Here we discuss each cluster in terms of composite flux patterns of lower layer and associated atmospheric circulation. The composite $\vec{Q}$, $\vec{Q}_L$, and geopotential height maps for each cluster are constructed by averaging the cases of each cluster. Figures 13a and 13b show composites of water vapor flux of the cluster A1 for a) total flux and b) lower level, respectively. Figures 13c and 13d represent the same as Figs. 13a and 13b but for A2. Compositted total water vapor flux patterns (Figs. 13a and 13c) overlap with the composite of 500 hPa height, while those of lower flux patterns (Figs. 13b and 13d) overlap with 850 hPa height fields. Major differences of the flux pattern between these two figures are noted around North China. Over North China, the northward flux of A1 is stronger than A2, which may be

Table 2. The days of heavy precipitation cases and their classified clusters. The fourth column indicates Taklimakan Precipitation (unit is millimeters).

Year	Month	Day	Precip.	Cluster
1980	August	26	3.1	A2
1981	July	5	8.6	H
1981	July	30	3.2	E
1981	July	31	3.6	E
1981	August	4	4.1	E
1981	August	22	3.8	A1
1982	August	27	3.8	A1
1982	August	28	4.2	A1
1983	August	4	4.0	B
1984	July	9	3.1	G
1984	July	10	3.8	G

related to seasonal change, since A1 appears more frequently in July than other months, while A2 appears less in July. This feature is consistent with the previous works (*e.g.*, Lau *et al.*, 1988) which show moisture from the south generally penetrates into the northernmost part of the Chinese Plain in July. Atmospheric circulation patterns (500 hPa geopotential height) corresponding to clusters A1 and A2 are also presented in Fig. 13. A broad trough exists around 80°E–100°E for cluster A1, while for A2, a weak ridge is located over this region. A high-pressure system appears over Central Asia in the 850 hPa height of cluster A1, while it does not appear in that of A2. Focussing on Figs. 13a and 13b, vertical inclination of a trough is seen around Mongolia. Namely, in Fig. 13b, a weak trough at 850 hPa height is seen around 95°E–110°E, which seems to be related with the upper level (500 hPa height) westward trough mentioned above. These patterns seem to show a developing baroclinic wave, which may relate to some precipitation events.

Average daily precipitation of cluster A1 (0.3 mm) exceeds that of A2 (0.2 mm). This result, that averaged precipitation of A1 exceeds that of A2, seems to consistent with the trough around Mongolia in the composite atmospheric circulation patterns of A1 mentioned above.

For clusters B and C, moisture flux to the Taklimakan Desert is related with the westerly flow, not with the monsoon flow. The atmospheric circulation pattern (Fig. 14) composited for cluster B shows that troughs exist at around 50°N/60°E and 37°N/110°E. The atmospheric circulation pattern for cluster C (not shown) is similar to that of B, but no trough exists around 60°E. Composite flux pattern of cluster D (Fig. 9d) has a complicated structure. Anticyclonic circulation appears over the Tibetan Plateau. This cluster only includes four cases and this pattern seldom brings rain to the desert.

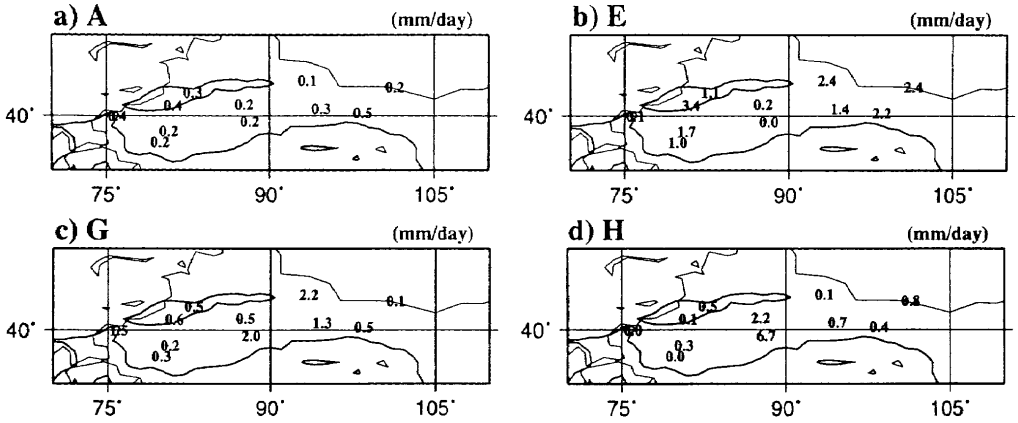

Fig. 11. Composite maps of precipitation of each station for cluster a) A, b) E, c) G and d) H.

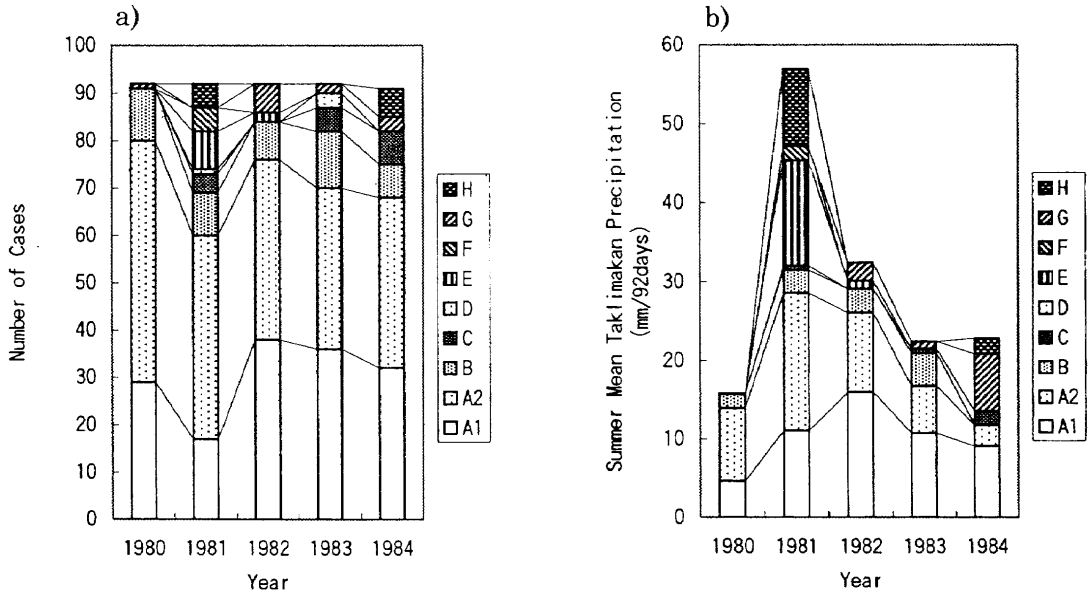

Fig. 12. a) Number of classified clusters for each year. b) Contribution of precipitation caused by each cluster to each year's total summer precipitation.

Strong water vapor flux from the south is found over the Tibetan Plateau and Gobi Desert in cluster E (Fig. 9e). Figure 15 depicts a composite height for 500 hPa overlapped with total moisture flux, and a composite height for 850 hPa with a lower layer moisture flux composite for cluster E. A low-pressure system (40°N/100°E) over the eastern part of the desert at 850 hPa level is associated with the northwestward or westward flux around the low-pressure system. The relationship between the easterly and the precipitation around the southeastern part of Taklimkan Desert has already been pointed out (Zhang and Deng, 1987; Yatagai and Yasunari, 1993). The easterly and precipitation may be related with this low pressure system. In the precipitation pattern related with cluster E (Fig. 11b), relatively strong precipitation is observed around the low-pressure system. This low-pressure system seems to be coupled with the upper deep trough extending from NNE to SSW around 80°E. In this pattern, the Taklimakan Desert is located in front of the trough. Therefore, this circulation pattern may cause heavy precipitation by providing unstable atmospheric conditions and moisture supply.

In the cluster F pattern (Fig. 9f), a westward flux is dominant over Mongolia. A northward flux can be seen over the eastern Taklimakan Desert. Composite water vapor flux patterns of cluster F overlapped with circulation patterns are displayed in Fig. 16. A strong northwestward flux, which is carried by anticyclonic circulation situated in the middle part of China, is seen over the Tibetan Plateau. At the lower level (not shown), moisture comes from the east. This circulation and moisture transport pattern seems to be very exceptional.

Clusters G and H also represent southerly moisture flux related to the southerly flow over the Tibetan Plateau, and they resemble each other. Figure

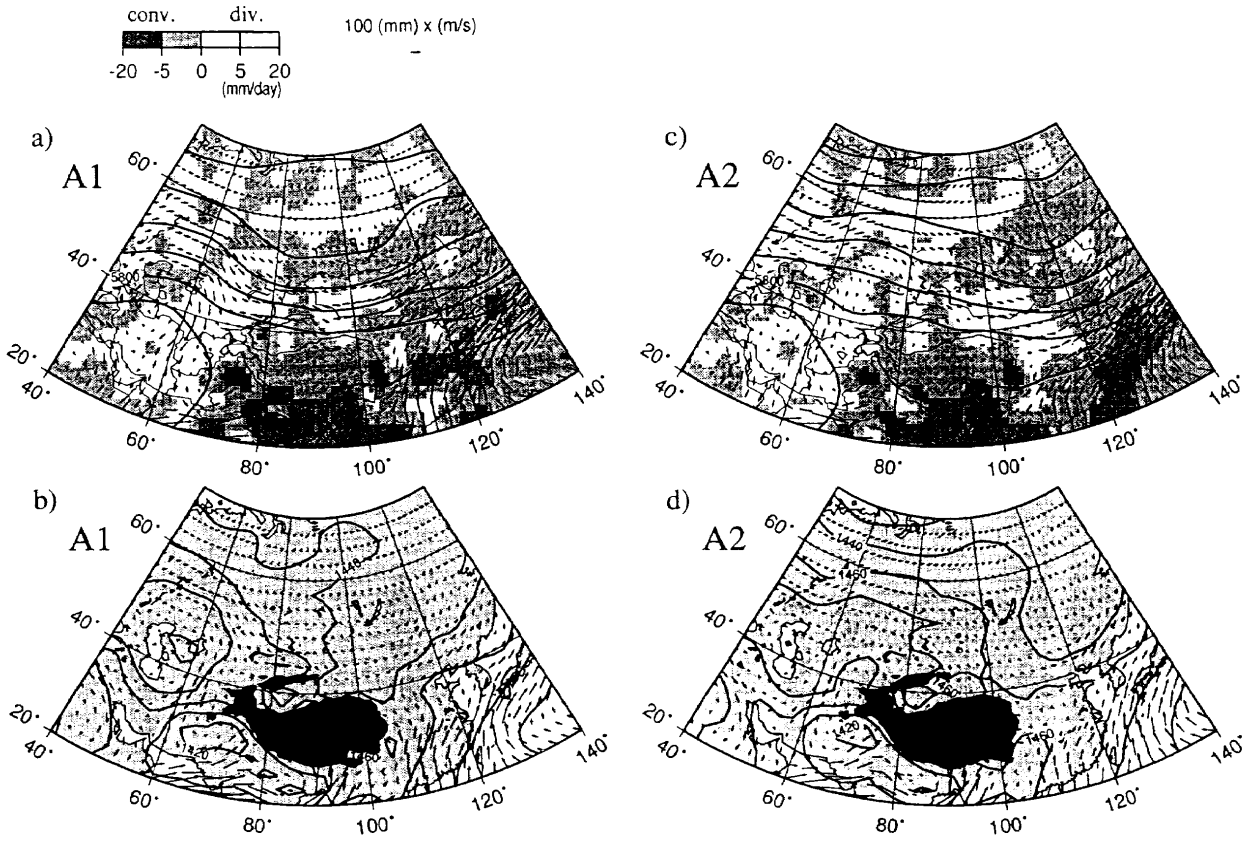

Fig. 13. Composite maps of atmospheric circulation fields for a) 500 hPa geopotential height and the total water vapor flux pattern of A1. Shaded area indicates convergence. Contour interval is 50 gpm, b) for 850 hPa geopotential height with the lower level water vapor flux pattern of A1. Contour interval is 20 gpm. Black area is Tibetan Plateau (above 3,000 m). c) The same as a) but for cluster A2. d) The same as b) but for cluster A2.

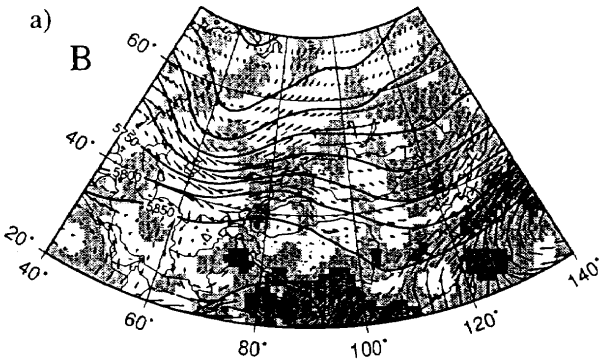

Fig. 14. Same as Fig. 10a but for cluster B.

17 presents the circulation patterns of cluster G for a) 500 hPa and b) 850 hPa. A large anti-cyclonic circulation appears over Central Asia. This high-pressure system and ridge are also seen in the composite pattern of cluster H in Fig. 18 (lower level not shown). A trough is located along 100°E, extending further to western Tibet, in cluster G. A trough also appears along 75°E, and a weak ridge and a high-pressure system (850 hPa) exist around 100°E. In Fig. 18, a strong convergence zone is seen around 100°E～/35°N, and may be related with a Mei-yu front. At the lower level composite of cluster G, a westward moisture flux associated with the low pressure around 100°E/40°N is seen. This is basically the same circulation pattern in the lower layer as in cluster E. Interestingly, cluster E primarily appeared in 1981, while cluster G did not (Table 1). Further, cluster H contains the cases of 1981 and 1984 and the heaviest precipitation case is included in this cluster. The composite precipitation pattern of G and H (Figs. 11c and 11d) show that much rainfall is observed around 40°N/90°E. This is a little difference from that of cluster E (Fig. 11b) which shows relatively little rainfall.

5.3 Water vapor budget

To examine the water vapor source for precipitation in the Taklimakan Desert, the water vapor budgets of clusters A, B, E and G are computed as shown in Fig. 19. The budget of cluster A resembles that of the seasonal mean (Fig. 2). For cluster B, northwesterly flux flow brings much moisture to the

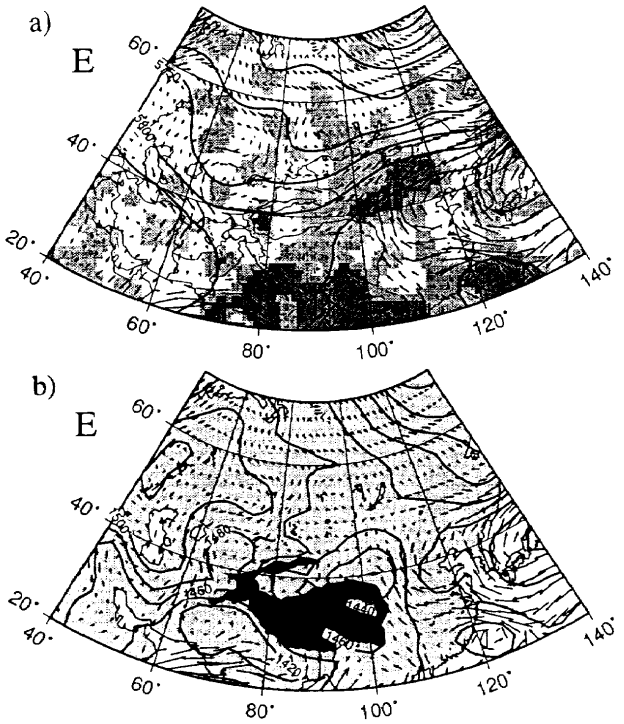

Fig. 15. Composite maps of atmospheric circulation fields, a) for 500 hPa geopotential height of cluster E with the water vapor flux pattern of E. Shaded area indicates convergence. Contour interval is 50 gpm. b) Composite maps for 850 hPa geopotential height of cluster E with the lower level water vapor flux pattern of E. Contour interval is 20 gpm.

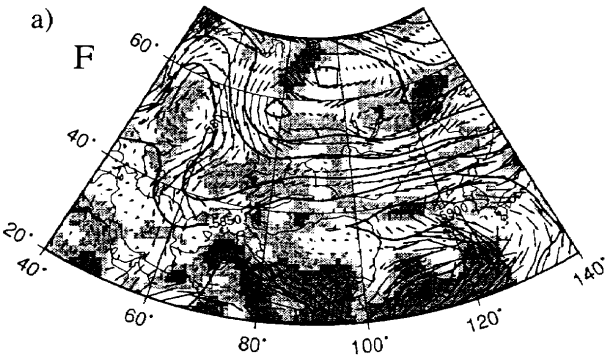

Fig. 16. Same as Fig. 10a but for cluster F.

desert, and it outflows to the eastward and southward. As a net balance, this box region shows a very weak convergence for this cluster. The budget of cluster C (not shown) depicts a similar structure to that of B, but this box region shows a weak divergence (-1.5×10^{12} kg/day). This cluster only shows total divergence, which is consistent with the fact that this cluster is seldom related to heavy precipitation.

The budgets of clusters E and F resemble each

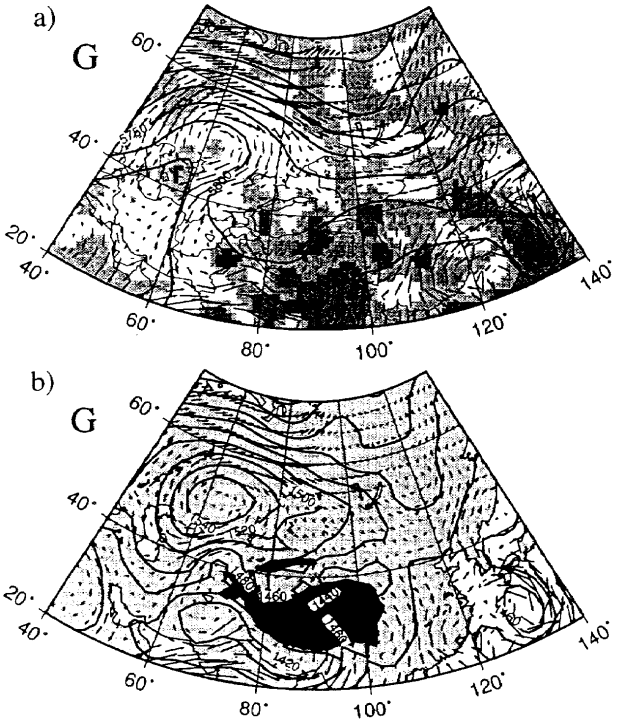

Fig. 17. Same as Fig. 12 but for cluster G.

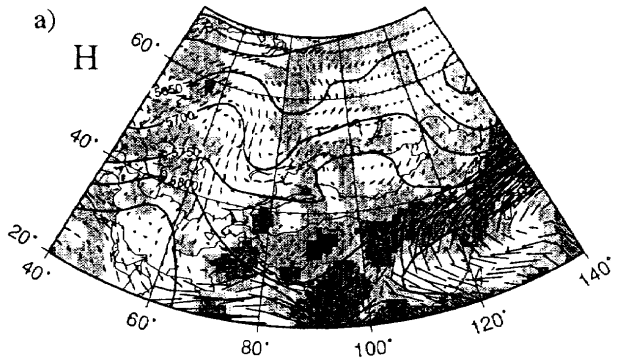

Fig. 18. Same as Fig. 10a but for cluster H.

other, but convergence of E (3.5×10^{12} kg/day) is stronger than that of F (1.2×10^{12} kg/day). This may be related to the fact shown in Fig. 10, which indicates averaged precipitation of cluster F is much less than that of E. A remarkably strong southerly flow appears in Fig. 19c. The inflow from the south side exceeds the outflow from the north side. Moisture also enters from the west, while little outflow is seen in the east. This very weak transport at the east side is attributed to the vertical shear of moisture flux there. Specifically, the upper level eastward (northeastward) moisture flow and lower level easterly moisture flow canceled each other as shown in Fig. 15.

Clusters G and H resemble each other, we show only the budget of cluster G. Interestingly, most of the moisture come from the south and converges

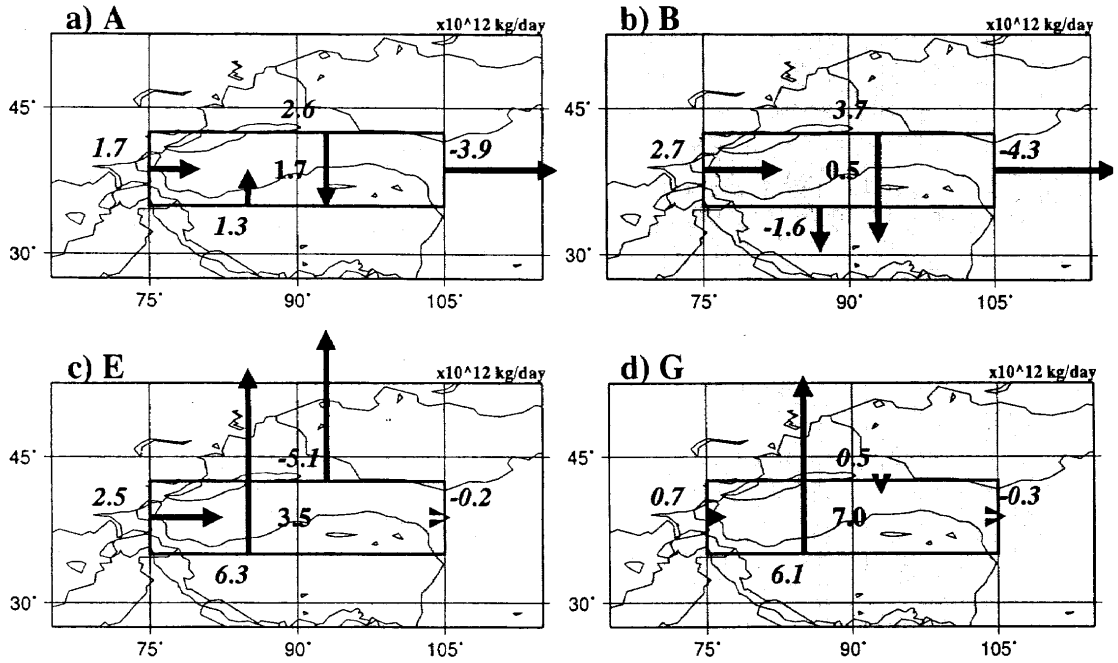

Fig. 19. The budget of water vapor flux around the Taklimakan Desert for clusters a) A, b) B, c) E and d) G. Legends are the same as those of Fig. 2. Each net budget value corresponds to a) 0.8, b) 0.3, c) 1.6 and d) 3.2 mm/day.

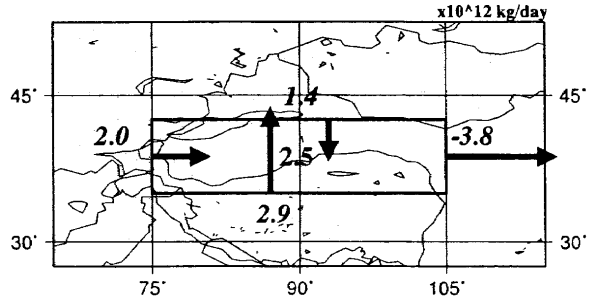

Fig. 20. The mean budget of water vapor flux around the Taklimakan Desert for the summer of 1981. Details are the same as those of Fig. 2. The net value corresponds to 1.2 mm/day.

very strongly. The box mean convergence of G amounts to 7.0×10^{12} kg/day, which is the strongest value of all the discussed clusters.

The southerly flux suggested in Figs. 19c and 19d does not appear every year. Since this analysis clarified that such cases occurred frequently in 1981, the water vapor budget averaged for the 1981 summer is presented in Fig. 20 for comparison with Fig. 2. The larger inflow from the southern boundary in 1981 would be largely due to the frequent appearance of the above mentioned situations. It is clearly seen that, in 1981, inflow from the southern boundary exceeded that of the 5-year mean, while the northern boundary inflow is weaker.

6. Discussion

By classifying water vapor transport, two major categories have been noticed in terms of major water vapor transport around the Taklimakan Desert, *i.e.*, northwesterly moisture flux patterns (A, B and C) and strong southerly moisture flux patterns (E, F, G and H). The northwesterly patterns account for 417 cases (90.7 %), and the southerly patterns, for 38 (8.3 %). Southerly moisture flux patterns appeared more frequently in wet years. In particular, 20 cases among the 38 cases of southerly flux patterns appeared in 1981. Of the total five-year Taklimakan precipitation, 74.3 % was related to the northwesterly patterns, and 24.5 %, to the southerly patterns. In 1981 and 1984, the percentage of the latter reached nearly fifty percent.

It has been known that precipitation in the Taklimakan Desert is mainly associated with disturbances embedded in the mid-latitude westerly circulation (Zhang and Deng, 1987). Recent observational studies of precipitation in the easternmost part of the Taklimakan Desert have also pointed out that the precipitation there occurs under unstable atmospheric conditions related to westerly disturbances (Itano, 1997, 1998). The study concerning the relationship between the interannual variation of summer precipitation of the Taklimakan Desert and atmospheric circulation also pointed out that the wet year for the desert is related to the westerly trough extending around 90°E and the ridge around Central Asia (Yatagai and Yasunari, 1995).

The present study has proved to be consistent with those studies. The atmospheric circulation patterns associated with the southerly flux pattern (Figs. 15, 16, 17 and 18) represent the combination of the deep trough and ridge around Central Asia. Further, the atmospheric circulation pattern associated with cluster A1 shows the trough extending to the desert. Cluster A1 contains more heavy precipitation cases than A2, and average precipitation of A1 exceeds that of A2. These results are consistent with the above studies.

The deep trough extending southwestward over Central Asia is likely to provide a very favorable condition for supplying moisture from the south over the Tibetan Plateau into the mid-latitude arid and semi-arid regions. This circulation is likely to accompany the low-pressure system in the lower troposphere around the eastern part of the Taklimakan Desert. As mentioned above, the existence of the trough has also been regarded as a condition for precipitation. However, a strong southerly flux over the Tibetan Plateau has not been noted before. According to Luo and Yanai (1983), the eastern Tibetan Plateau acts as a "giant chimney" funneling water vapor from the lower to the upper troposphere. Therefore, if the trough and ridge are located in the right place, moisture from the south may flow over the arid region, which is located northward over the Plateau.

Unfortunately, the method used here cannot solve the problem of water origin, nor how much water vapor coming from the south really falls as precipitation. In the future, it would be worth examining the relation of the southerly flux over the Plateau and heavy precipitation in the desert.

It is notable that the southerly circulation pattern does not occur so frequently, representing no more than 20 % of the total cases with a large year-to-year variability. However,this pattern is related with heavy precipitation. An El Niño/Southern Oscillation (ENSO) event occurred in 1982 and 1983. Wang and Li (1990) and Yatagai and Yasunari (1995) pointed out that the Loess Plateau has less precipitation in the ENSO years and weak monsoon years. However, the present study shows that the precipitation over the Taklimkan Desert did not create a special signal in 1982 and 1983 compared with other years. Comparing Figs. 17a and 17b, the appearance of cluster E seems to be more important than that of G and H. Further studies using longer period dataset is necessary to understand the physical mechanism between global-scale climate change and moisture transport around the arid region in the interior of the Eurasian Continent.

7. Summary

Water vapor transport and its divergence or convergence are examined over the interior of the Eurasian Continent, particularly with respect to precipitation events in the Taklimakan Desert, where the mid-latitude westerly flow and southerly monsoon flow penetrate and interact each other. The water vapor flux is computed using the objective re-analysis data of ECMWF.

In the vertically integrated water vapor transport fields, the northern parts of China and Mongolia receive water vapor from the northwest in the summer mean field. One of the water vapor sources is likely to be in Western Siberia, including the inland seas and large lakes. The Taklimakan Desert also receives water vapor transported along the eastern periphery of the Tianshan Mountains from the northwest in the lower troposphere.

Precipitation and associated atmospheric circulation fields are examined based on daily data over these arid and semi-arid regions, since episodic precipitation within a few days sometimes determines the annual total amount. Therefore, the daily water vapor flux field is analyzed with respect to precipitation variability. Here, the daily mean water vapor transport patterns are classified using cluster analysis.

The 460 cases (days) in the summer of five years (1980–1984) are classified into eight clusters. The total column water vapor flux, the lower level water vapor flux (surface to 700 hPa), the regional precipitation, and the geopotential height at 850 hPa and 500 hPa are then composited for each cluster. Two major categories of water vapor flux patterns have been deduced. Northwesterly moisture flow dominates in the three patterns, representing more than 90 % of the total cases, while strong southerly moisture flux is apparent in four other patterns (8.3 % of total cases). The former basically contributes to the mean field.

The latter pattern is characterized by the strong water vapor flux observed over the Tibetan Plateau. Moisture from the south is also seen at the eastern part of the Taklimakan Desert in the lower level, flowing along the northeast periphery of the Plateau. In this pattern, a northerly flux also appeared over the Desert, but it seems to be weak compared to the southerly flow. In this case, a deep trough extends from NNE to SSW around 80°E, and a high pressure system exists to the west (*i.e.*, over Central Asia). Around the Taklimakan Desert, the 850 hPa height is relatively low, which is responsible for the lower level easterly flow bringing much water vapor from the south. This type is associated with heavy precipitation, mainly in the eastern part of Taklimakan.

Finally, the interannual variability of occurrence of these clusters and the total water vapor transport are investigated, focusing on strong precipitation and associated atmospheric circulation patterns. The southerly flux pattern frequently oc-

curred in the wet years. This pattern occurs with an upper level trough to the north or northwest of the Taklimakan Desert coupled with a ridge over Central Asia. These southerly flux patterns are associated with heavy precipitation, which occur only in the wet years. This immediately implies that the water vapor flux coming over the Tibetan Plateau is strongly related to intensive precipitation, which determines the moisture budget around the desert and its large interannual variability.

Acknowledgments

This study was conducted as part of the Ph.D thesis of the first author in the Institute of Geoscience, University of Tsukuba. The authors would like to thank Prof. F. Kimura, Prof. K. Kotoda, Dr. H.L. Tanaka and Dr. K. Kai of the Institute of Geoscience, University of Tsukuba, for discussions and constructive comments. We are also grateful to Dr. T. Oki, Institute of Industrial Science, University of Tokyo, for providing a computer program for the water vapor flux calculation. Thanks are additionally extended to Dr. R. Suzuki for permitting us to use the computing program and the many comments on cluster analysis. We thank Dr. J. Matsumoto, University of Tokyo and anonymous referees, for constructive comments in the revision of this paper.

Part of this work was supported by the National Institute Post Doctoral Fellowship of the Research Development Corporation of Japan (JRDC). Most of the figures are drawn using the GMT System (Wessel and Smith, 1991).

References

Akiyama, T., 1973: The large-scale aspects of the characteristics of the Baiu front. *Pap. Meteor. Geophys.*, **24**, 157–188.

Asakura, T., 1973: Transport and source of water vapor in the northern hemisphere and monsoon Asia. *Water Balance of Monsoon Asia*, Yoshino, M.M. ed., Univ. Tokyo Press, 131–151.

Bengtsson, L., M. Kanamitsu, P. Kallberg and S. Uppala, 1982: FGGE 4-dimensional data assimilation at ECMWF. *Bull. Amer. Meteor. Soc.*, **63**, 29–43.

Bryan, F. and A. Oort, 1984: Seasonal variation of the global water balance based on aerological data. *J. Geophys. Res.*, **89**, 11717–11730.

Everitt, B., 1993: *Cluster analysis*, Third Edn. Edward Arnold, 170pp.

Goff, J.A. and S. Gratch, 1946: Low-pressure properties of water — from 160 to 212°F. *Trans. Am. Heat. Vent. Eng.*, **52**, 95–121.

Itano, T., 1997: Rainfall over the arid area in the Northwestern China — An analysis during HEIFE —. *J. Meteor. Soc. Japan*, **75**, 851–865.

Itano, T., 1998: Synoptic disturbance and rainfall over the arid area in the Northwestern China. *J. Meteor. Soc. Japan*, **76**, 325–333.

Kato, K., H. Iwasaki and J. Matsumoto, 1992: A preliminary report on the water cycle around the arid and semiarid area in East Asia. *Tenki*, **39**, 408–413 (in Japanese).

Kato, K., 1993: Large-scale atmospheric condition around the arid region in China through warm season. *Proc. Intern. Symp. on HEIFE*, Kyoto Univ. Nov. 8–11, 1993, 69–78.

Kato, K., 1995: Large-scale and meso-scale atmospheric processes. Mitsuta, Y. ed., *Natural environment of the arid region*, *Meteor. Res. Note*, **184**, 13–46 (in Japanese).

Kitoh, A., K. Yamazaki and T. Tokioka, 1993: Summertime moisture flux in the desert regions of Western China. *J. Arid Land Studies*, **3**, 9–17 (in Japanese with English abstract).

Lau, K.M., G.J. Yang and S.H. Shen, 1988: Seasonal and intraseasonal climatology of summer monsoon rainfall over east Asia. *Mon. Wea. Rev.*, **116**, 18–37.

Luo, H. and M. Yanai, 1983: The large-scale circulation and heat sources over the Tibetan Plateau and surrounding areas during the early summer of 1979. Part I: Precipitation and kinematic analysis. *Mon. Wea. Rev.*, **111**, 922–944.

Murakami, T., 1959: The general circulation and water-vapor balance over the Far East during the rainy season. *Geophy. Mag.*, **29**, 131–171.

Murakami, T., T. Nakazawa and J. He, 1984: On the 40–50 day oscillation during the 1979 Northern Hemisphere summer. Part II: Heat and moisture budget. *J. Meteor. Soc. Japan.*, **62**, 469–484.

Oki, T., K. Musiake, H. Matsuyama and K. Masuda, 1995: Global atmospheric water balance and runoff from large river basins. *Hydrological Processes*, **9**, 655–678.

Suzuki, R. and T. Kawamura, 1987: Characteristics of the wind systems under typical summer conditions in central Japan. *Tenki*, **43**, 715–722 (in Japanese).

Suzuki, R., 1990: The influence of daytime heating and nocturnal cooling on surface airflow patterns over central Japan. *Int. J. Climatology*, **11**, 297–313.

Tagami, Y., 1982: Macro-scale airflow patterns and distributions of climatic elements in the Japanese islands. *Geogr. Rev. Japan*, **55A**, 799–813 (in Japanese with English abstract).

Wang, W.-C. and K. Li, 1990: Precipitation fluctuation over semi arid region in Northern China and the relationship with El Niño/Southern Oscillation. *J. Climate*, **3**, 769–783.

Wessel, P. and W.H.F. Smith, 1991: Free software helps map and display data. *EOS Trans. AGU*, **72**, 441, 445–446.

Yatagai, A. and T. Yasunari, 1993: The precipitation and water vapor transport over and around the arid and semi-arid regions of China. *Proc. Intern. Symp. on HEIFE*, Kyoto Univ. Nov. 8–11, 1993, 51–61.

Yatagai, A. and T. Yasunari, 1995: Interannual variations of summer precipitation in the arid/semi-arid regions in China and Mongolia: Their regionality and relation to the Asian summer monsoon. *J. Meteor. Soc. Japan*, **73**, 909–923.

Yoshino, M. and G.-Y. Chen, 1975: *Rain and climate of China*, Taimeido, 216pp. (in Japanese)

Yoshino, M., 1991: Wind and Rain in the Desert Region of Xinjiang, China. *J. Arid Land Studies*, **1**, 1–15 (in Japanese with English abstract).

Zhang, J.B. and Z.-F. Deng, 1987: *Introduction to precipitation in Xinjiang.* Meto. Publ. Beijing, 400pp (in Chinese).

ユーラシア大陸内陸の乾燥・半乾燥地域における夏季の水蒸気輸送と降水の変動

谷田貝亜紀代
（宇宙開発事業団地球観測データ解析研究センター）
安成哲三
（筑波大学地球科学系）

ユーラシア大陸内陸の乾燥地域周辺は、砂漠化の問題が生じている地域であり、それらの地域の水循環の変動を、全球、大陸スケールの気候変動とあわせて明らかにすることは不可欠である。内陸の乾燥地域においても、夏季にしばしば強い降水がみられるが、それに関連する水蒸気輸送場は、若干の事例解析があるのみで、気候変動と関連づけて研究した例はほとんどない。そこで、本研究はまず、ユーラシア大陸内陸の乾燥地域周辺における夏季の水蒸気輸送とその収束発散場をヨーロッパ中期予報センター (ECMWF) の再解析データを5年間 (1980–1984年) について使用して調べた。

夏季平均の鉛直積分された水蒸気フラックス場は、モンゴルと中国北部には北西方向からの水蒸気が輸送されることを示す。平均場では、これらの地域の水蒸気源は西シベリアと、さらにその西方向である。大陸のうち最も乾燥したタクラマカン砂漠への、対流圏下層の水蒸気輸送場をみると、この地域の北西方向からの水蒸気が天山山脈の東側をまわりこむように水蒸気が輸送されていることがわかった。

次にタクラマカン砂漠の降水と日平均水蒸気輸送場の関係を統計的に調べた。タクラマカン砂漠周辺の全層水蒸気フラックス場をクラスター分析により、まず8パターンに分類した。次に、日降水量と大気循環場をこれらのクラスターごとに合成した。全体の約9割は、平均場に似て、北西からの輸送に関係したパターンであり、このケースの場合、上空にトラフが存在する時に降雨がみられる。

しかし、時折、チベット高原を超えて南から水蒸気が流入し、同時にタクラマカン東部 (チベット高原の北東側) の下層で東から水蒸気が入り込むことがあり、このパターンはタクラマカンの強い降水と関係している。大気循環場の特徴として、500 hPa等圧面高度の合成図をみると、南西方向に深く伸びたトラフがタクラマカンの北側に出現し、これと同時に中央アジアではリッジが現れる。東風の見られるタクラマカン東部には下層に低気圧が存在する。このケースは、全体の10％以下であるが、出現は多雨年に偏り、多雨年 (1981, 1984) の夏季降水量の約半分がこのような循環場でもたらされている。